Atmos. Meas. Tech., 3, 1155–1174, 2010
www.atmos-meas-tech.net/3/1155/2010/
doi:10.5194/amt-3-1155-2010

Atmospheric Measurement Techniques

The effect of horizontal gradients and spatial measurement resolution on the retrieval of global vertical NO_2 distributions from SCIAMACHY measurements in limb only mode

J. Puķīte[1], S. Kühl[1], T. Deutschmann[2], S. Dörner[1], P. Jöckel[1,*], U. Platt[2], and T. Wagner[1]

[1]Max Planck Institute for Chemistry, J. J. Becher Weg 27, 55128 Mainz, Germany
[2]Institute of Environmental Physics, University of Heidelberg, Im Neuenheimer Feld 229, 69120 Heidelberg, Germany
[*]now at: Deutsches Zentrum für Luft- und Raumfahrt (DLR), Institut für Physik der Atmosphäre, Oberpfaffenhofen, 82234 Weßling, Germany

Received: 6 April 2010 – Published in Atmos. Meas. Tech. Discuss.: 11 May 2010
Revised: 18 August 2010 – Accepted: 23 August 2010 – Published: 30 August 2010

Abstract. Limb measurements provided by the Scanning Imaging Absorption spectroMeter for Atmospheric CHartographY (SCIAMACHY) on the ENVISAT satellite allow retrieving stratospheric profiles of various trace gases on a global scale. Combining measurements of the same air volume from different viewing positions along the orbit, a tomographic approach can be applied and 2-D distribution fields of stratospheric trace gases can be acquired in one inversion. With this approach, it is possible to improve the accounting for the effect of horizontal gradients in the trace gas distribution on the profile retrieval. This was shown in a previous study for the retrieval of NO_2 and OClO profiles in the Arctic region near the polar vortex boundary.

In this study, the tomographic retrieval is applied on measurements during special limb-only orbits performed on 14 December 2008. For these orbits the distance between consecutive limb scanning sequences was reduced to $\sim$3.3° of the orbital circle (i.e. more than two times with respect to the nominal operational mode). Thus, the same air volumes are scanned successively by more than one scanning sequence also for midlatitudes and the tropics. It is found that the profiles obtained by the tomographic 2-D approach show significant differences to those obtained by the 1-D approach. In particular, for regions close to stratospheric transport barriers (i.e. near to the edge of the polar vortex and subtropical transport barrier) up to 50% larger or smaller NO_2 number densities (depending on the sign of the gradient along the line of sight) for altitudes below the peak of the profile (around 20 km) are obtained.

The limb-only measurements allow examining the systematic error if the horizontal gradient is not accounted for, and studying the impact of the gradient strength on the profile retrieval on a global scale. The findings for the actual SCIAMACHY observations are verified by sensitivity studies for simulated data for which the NO_2 distributions to be retrieved are known in advance. In addition, the impact of the horizontal distance between consecutive limb scanning sequences on the quality of the tomographic 2-D retrieval is investigated and a possibility to take into account the horizontal gradients by an interpolation approach is studied.

Correspondence to: J. Puķīte
(janis.pukite@mpic.de)

1 Introduction

Measurements in satellite limb geometry (i.e. tangential view with respect to the Earth surface) offer the opportunity to acquire height resolved profile information of various atmospheric parameters. This is achieved by measuring light from air masses at different tangent heights (THs) in a vertical scanning sequence and combining the measurements of all THs in an inversion algorithm. Several retrieval algorithms exist, for ENVISAT-SCIAMACHY limb measurements of scattered sunlight (see for example Sioris et al., 2004; Rozanov et al., 2005; Kühl, 2005; von Savigny et al., 2005; Sioris et al., 2006; Puķīte et al., 2006; Kühl et al., 2008). Further, it is possible to acquire not only vertically but

Published by Copernicus Publications on behalf of the European Geosciences Union.

also horizontally resolved information on the number density field if the backscattered light of the same air volume is measured at different sites along the orbit. In these cases, the spatial correlation between these measurements can be taken into account and a tomographic (2-D) approach can be applied (Puķīte et al., 2008), i.e. the measurements from several consecutive SCIAMACHY limb scanning sequences are combined in one inversion. This approach improves the profile retrieval by taking into account horizontal gradients of the trace gas distribution in flight/viewing direction and requires that the sites, where the measurement sequences are performed, are close enough that the probed air masses partially overlap.

It is important to mention that also tomographic approaches for satellites measuring infrared emission exist, for MIPAS on ENVISAT (see e.g. Carlotti et al., 2001; Ridolfi et al., 2004; Steck et al., 2005; Carlotti et al., 2006). Also, the infrared channels of OSIRIS are specifically designed for tomographic retrievals, although they are mainly used for measurements of terrestrial airglow emissions and not for limb-scattered radiation (see Degenstein et al., 2003 and references on airglow emission tomography therein).

The SCIAMACHY instrument on the ENVISAT satellite operates in a near polar sun synchronous orbit with an inclination from the equatorial plane of ∼98.5°. It performs one orbit in ∼100 min with an equator crossing time of 10:00 for the descending node. In the normal operation mode, the satellite probes the atmosphere at the day side of Earth in alternating sequences of nadir and limb measurements. Vertical limb scans for one scanning sequence are performed with approx. 3.3 km elevation steps at the tangent point (TP) in flight direction. The cross track swath is 960 km at the TP and consists of up to 4 pixels for the UV/VIS spectral range. The field of view (FOV) is 0.045° in elevation and 1.8° in azimuth. This corresponds to approx. 2.5 km in vertical direction and 110 km in horizontal direction at the TP, respectively. For nominal orbits (with alternating limb and nadir measurements) the distance between TPs of consecutive limb scanning sequences is 7.5° of the orbital cycle (i.e. ∼830 km). SCIAMACHY measures in the UV-VIS-NIR spectral range from 240 to 2380 nm with a spectral resolution of approx. 0.25 to 0.55 nm in the UV-VIS range. More instrumental details can be found in Bovensmann et al. (1999).

In Puķīte et al. (2008), the 2-D tomographic approach was applied for the most northern parts of SCIAMACHY orbits where no nadir measurements are performed. Therefore the distance between the satellite positions of consecutive limb scanning sequences is reduced to ∼3.3° (corresponding to approx. 370 km along the Earth's surface), which allows for a tomographic retrieval approach. It was found that, if the horizontal inhomogenity in the distribution of the considered species is not properly accounted for (i.e. if the retrieval was performed separately for every scanning sequence by the 1-D approach), typical errors of 20% for NO_2 and up to 50% for OClO around the altitude of the profile peak can arise for

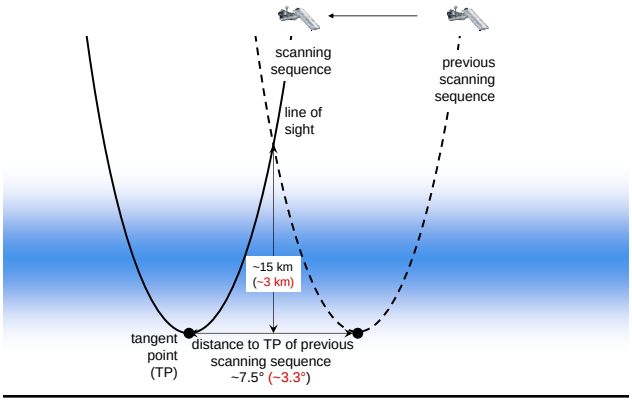

Fig. 1. Spatial overlap of the LOSs of two consecutive scanning sequences (for the same TH). If the distance between their TPs is 7.5° (nominal SCIAMACHY orbits), they intersect ∼15 km above the TH indicating rather poor spatial overlap. On the other hand, for a distance of 3.3° (full limb orbits), they cross ∼3 km above the TH.

measurements close to the Arctic polar vortex boundary in boreal winter. However, the 2-D tomographic approach can correct for most of these errors by taking into account the information from all scanning sequences that probe a particular air volume.

For the normal operational mode with 7.5° distance between consecutive limb scanning sequences, the spatial overlap of the scanned air masses is very weak: i.e. the line of sight (LOS) for the actual tangent point crosses the point of half distance to the tangent point of the previous limb scanning sequence with a difference in altitude of almost 15 km (see Fig. 1), therefore not allowing a 2-D tomographic retrieval. Under an operational change request made by the authors, seven consecutive SCIAMACHY orbits (nr. 35499–35505) on 14 December 2008 were performed in limb mode only (i.e. without nadir scans between consecutive limb scanning sequences) for investigating the horizontal gradient effect on the 2-D tomographic profile retrieval globally. Therefore, the distance between two consecutive limb scanning sequences is reduced to ∼3.3° for the whole orbit, and the LOS for the actual tangent point crosses the point of half distance to the tangent point of the previous limb scanning sequence with a difference in altitude of only 3 km (as indicated in Fig. 1). This reduced spatial distance between consecutive limb scanning sequences by slightly more than a factor of two for the whole orbit provides valuable information about possibilities to correct for horizontal gradients also at tropical and midlatitude regions.

In Sect. 2 we describe the retrieval algorithms which are applied for the retrieval of the vertical NO_2 distribution in Sect. 3. Additionally to the 1-D and 2-D approach applied in Puķīte et al. (2008) we also study a possibility to apply

an interpolation approach. It assumes that the number density in the regions between the consecutive limb scanning sequences changes linearly. In Sect. 4, the 1-D and 2-D retrieval approaches are applied to simulated measurements to investigate the performance and limitations of the 2-D and the interpolation approaches for different gradient strengths. Also, an estimate for the optimal distance between consecutive limb scanning sequences to account for the typical horizontal gradients of the NO_2 concentration is derived from the sensitivity studies. Section 5 draws some conclusions.

2 Retrieval algorithm

All retrieval approaches, for which the obtained profiles are compared in the following, are based on a two step method developed in our group (the remote sensing group of the Max Planck institute for Chemistry in Mainz and also two members of the atmospheric physics group from the Institute of Environmental Physics in Heidelberg) for the retrieval of stratospheric trace gas distributions (NO_2, BrO and OClO) from SCIAMACHY limb measurements (Kühl, 2005; Puķīte et al., 2006; Kühl et al., 2008; Puķīte et al., 2008).

The first step, where slant column densities (SCDs), the integrated number density of the absorber along the light path, are derived from the SCIAMACHY limb spectra by Differential Optical Absorption Spectroscopy (DOAS, see e.g. Platt and Stutz, 2008), is common for all approaches. In particular, the same fit window (420–450 nm) and Fraunhofer reference spectrum at the TH of ∼42 km is applied. Further details of the NO_2 SCD retrieval are described in Kühl et al. (2008). In the second step, the retrieved SCDs are converted into vertical (for 1-D approach) and additionally horizontal (for 2-D approaches) number density profiles by the optimal estimation method (Rodgers, 2000). For all approaches radiative transfer modelling is performed with the fully spherical Monte Carlo radiative transfer model McArtim (Deutschmann, 2009), a successor of the RTM Tracy-II (Wagner et al., 2007), which was applied for the studies performed in Puķīte et al. (2008). The main difference between McArtim and Tracy-II is that in McArtim the separation between trajectory generation and weighting is not performed, i.e. the absorption is included in the trajectory generation. This increases calculation speed especially for cases with large optical depths. All features relevant for this study like the full sphericity option, and the 3-D box AMF concept are kept and do not affect the results. We study and compare three different approaches for the definition of the forward (and inverse) problem, which are described in the following subsections.

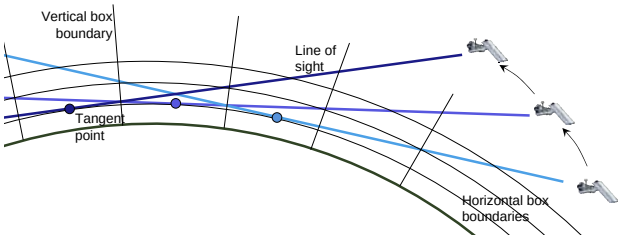

Fig. 2. Definition of the horizontal model space for the 2-D retrieval with respect to the tangent points of the scanning sequences. For illustration purposes, the LOS of only one measurement (for the same TH) per scanning sequence is shown.

2.1 1-D retrieval

First we perform a simple 1-D retrieval (Puķīte et al., 2006; Kühl et al., 2008), where every scanning sequence is retrieved separately, i.e. measured SCDs at different THs of one scanning sequence are used for the inversion. This 1-D method does not take into account the horizontal gradients in the retrieval, thus assuming horizontally homogeneous trace gas distributions in the atmosphere. SCDs of only one scanning sequence are inverted simultaneously in one inversion, applying 1-D box air mass factors (box AMFs). Therefore, the SCD S for every measurement position and viewing geometry g (i.e. TH) is described as a sum of products of box AMFs A and number densities n for boxes b_{alt} resolved in altitude alt:

$$S_{\mathrm{g}} = h \sum_{b_{\mathrm{alt}}} A_{\mathrm{g,b_{alt}}} n_{\mathrm{b_{alt}}} \tag{1}$$

h is the vertical extension of the boxes which is set to 3 km for this study.

2.2 2-D retrieval

For the 2-D approach, the retrieval algorithm as described in Puķīte et al. (2008) is applied: The trace gas SCDs are converted into vertical and horizontal number density distributions by a tomographic approach. SCDs of all scanning sequences and THs of one orbit are inverted simultaneously in one inversion applying 2-D box AMFs. The SCD at the measurement position and viewing geometry g is described as the sum of products of box AMFs and number densities for boxes $b_{\mathrm{alt,lat}}$, resolved in altitude alt and latitude lat:

$$S_{\mathrm{g}} = h \sum_{b_{\mathrm{alt,lat}}} A_{\mathrm{g,b_{alt,lat}}} n_{\mathrm{b_{alt,lat}}} \tag{2}$$

In the latitude dimension, boundaries of the boxes are defined approximately at the midpoint of the tangent points (TPs) of two consecutive scanning sequences as shown in Fig. 2.

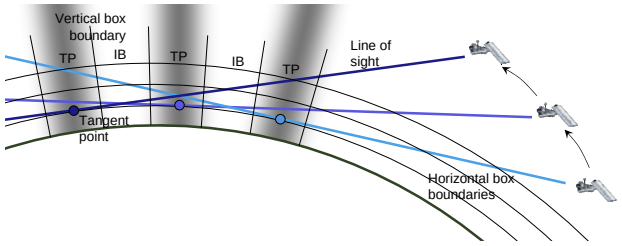

Fig. 3. Definition of the horizontal model space for the interpolation approach with respect to the tangent points of the scanning sequences if additional intermediate boxes are introduced. TP and dark shading indicates boxes around the tangent points, IB and white shading indicates the intermediate boxes. For illustration purposes, the LOS is shown for only one measurement per scanning sequence (at the same TH).

For the whole set of SCDs measured along the orbit, Eq. (2) can be written:

$$\boldsymbol{S} = h(\mathbf{A}\boldsymbol{n}) \tag{3}$$

where the matrix $\mathbf{A}$ consists of box AMFs for all measurement positions and all boxes along the orbit, and the vector $\boldsymbol{n}$ contains the number densities of all boxes.

2.3 2-D tomographic retrieval with interpolation constraint

For this approach, intermediate boxes are introduced in the latitude dimension with equal distances to each other and to the measurement TPs as shown in Fig. 3. Thus, for the interpolation approach, 2-D box AMFs are calculated on a finer latitude grid than the measurements occur. This allows for number density changes between the measurement sites in more than one step, so that a better agreement with the shape of a true number density change can be realized.

However, applying the 2-D tomographic retrieval with interpolation constraint it is necessary to eliminate the underdeterminancy that arises from the definition of the finer retrieval grid. This is done by describing the number density or box vertical column density, VCD (i.e. the product of the number density in the box and its vertical extension) in the additional boxes that are located in between the measurement TPs as a function of the number density (or VCD) of the boxes that are located at the TPs. Thus, only the number density for the boxes at the TPs is inverted directly.

The forward problem for the interpolation approach can be written as:

$$\boldsymbol{S} = h(\mathbf{A}_{\mathrm{TP}}\boldsymbol{n}_{\mathrm{TP}} + \mathbf{A}_{\mathrm{IB}}\boldsymbol{n}_{\mathrm{IB}}) = h(\mathbf{A}_{\mathrm{TP}} + \mathbf{A}_{\mathrm{IB}}\mathbf{X})\boldsymbol{n}_{\mathrm{TP}} \tag{4}$$

$\mathbf{A}_{\mathrm{TP}}$ and $\mathbf{A}_{\mathrm{IB}}$ are box AMFs for boxes at the TPs and in between, while $\boldsymbol{n}_{\mathrm{TP}}$ and $\boldsymbol{n}_{\mathrm{IB}}$ are the respective number densities. The matrix $\mathbf{X}$ describes the introduced relation (by interpolation) between $\boldsymbol{n}_{\mathrm{IB}}$ and $\boldsymbol{n}_{\mathrm{TP}}$. The number density for the boxes around the TPs, $\boldsymbol{n}_{\mathrm{TP}}$, is acquired by inversion like for the general 2-D approach. Thus no additional a-priori smoothing constraints like off-diagonal elements for the a-priori covariance matrix are necessary. In our study linear interpolation of number density is applied, although, in general, different kinds of interpolation may be defined by the matrix $\mathbf{X}$.

3 Application of the 2-D tomographic retrieval to the full limb orbits

In the following we compare the results for the NO_2 profile retrieval obtained by the different approaches described in Sect. 2 for the full limb orbits performed by SCIAMACHY on 14 December 2008.

3.1 Comparison between the results of the 1-D and 2-D approaches

To illustrate the differences in the vertical and horizontal NO_2 distribution retrieved by the 1-D and 2-D approach, the upper panels in Figs. 4 and 5 show the individual results for two of the full limb orbits. The absolute and relative differences between both retrievals are given in the middle and bottom panel, respectively.

As seen in the upper panels generally larger number densities of NO_2 are observed for the southern (summer season) hemisphere in contrast to lower number densities for the northern winter hemisphere, reflecting the seasonal dependence of NO_x chemistry and also the effect of stratospheric transport. In winter, less sunlight reaches the atmosphere decreasing the production of NO_x from N_2O, as well as increasing the abundance of reservoir species HNO_3 and N_2O_5 by denoxification (Brasseur and Solomon, 2005). Also, the peak altitude of the NO_2 profile varies with latitude and is larger for the tropics ($\sim$33 km) than for the polar regions ($\sim$25 km).

Strong differences between both retrievals occur at regions where strong horizontal gradients in the NO_2 field are observed. These regions are at the subtropics (10–30°) and at the midlatitudes (around 40–60°) in both hemispheres. In particular, in the summer hemisphere (i.e. the Southern Hemisphere in December), subtropical transport barriers strongly impact the stratospheric circulation patterns, affecting the latitudinal distribution of different trace gases in the stratosphere like e.g. H_2O and N_2O (Randel et al., 1993; Brasseur and Solomon, 2005), CH_4 (Russell et al., 1993) as well as aerosols (Trepte and Hitchman, 1992). On the other hand, in the winter hemisphere weaker gradients from the subtropics (i.e. 10° N) northwards occur because of rather effective mixing of air masses in this season with a stronger gradient only at the northern part of the midlatitudes due to the polar vortex. Since the main source of stratospheric NO_2 is the reaction of $O(^1D)$ with the long-lived tracer N_2O, these transport barriers also impact the distribution of NO_2.

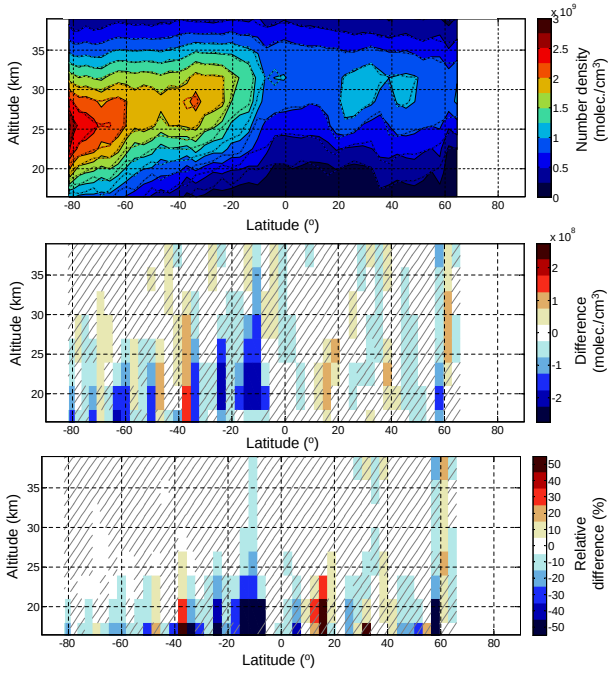

Fig. 4. Top panel: vertical and latitudinal distribution of NO_2 number density for orbit 35499 on 14 December 2008 retrieved by the 2-D approach (color plot with solid contourlines) and 1-D approach (dashed contourlines). Middle and bottom panels: absolute and relative difference between 1-D and 2-D approach for the retrieval boxes. Boxes, where the retrieval error is larger than the difference, are shaded by a diagonal pattern.

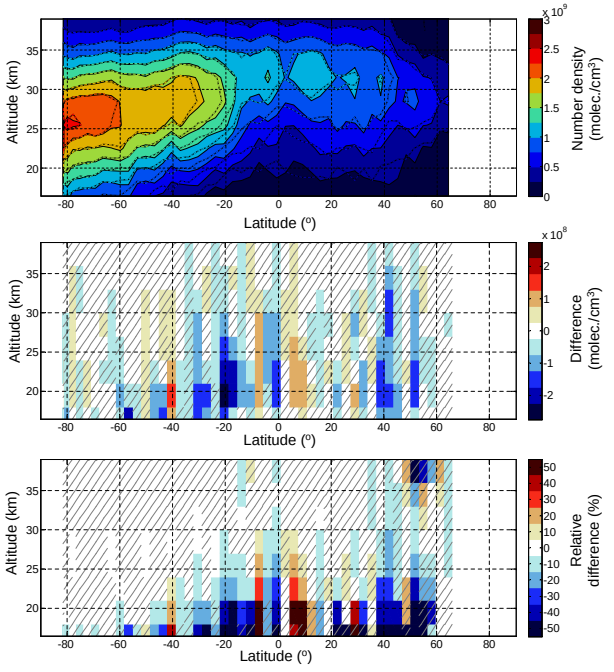

Fig. 5. Same as Fig. 4 but for orbit 35503.

Although also other factors control the abundance of the short lived species NO_2, a correlation to the strong gradients of N_2O observed by Randel et al. (1993) is found, e.g. across the tropical barrier the gradients of both tracers show an opposite trend for the same latitude interval.

Generally, the differences found between the 1-D and 2-D retrievals are in accord with the results in Puķīte et al. (2008): for regions at 10–30° S, around 60° S and at 40–60° N the number density of NO_2 decreases along the LOS towards the instrument (i.e. the gradient is negative). Therefore, since the instrument is more sensitive to the near limb side (i.e. the side between TP and the instrument), the lower number density field closer to the instrument dominates the observed SCDs and thus less NO_2 is retrieved by the 1-D approach. In contrast, for the northern subtropical region (10–30° N), where a weak positive gradient along the LOS is found, the instrument sees the higher number density field at the near limb side and, consequently under the assumption of a homogeneous NO_2 distribution in the 1-D forward model, a larger number density is retrieved wrongly for the location of the TH.

Note that also the statistical component of the retrieval error might cause part of the variations in the differences between 1-D and 2-D retrieval therefore the retrieval must have a certain precision in order to obtain a significant improvement by the 2-D approach. In particular for lower altitudes (below 20 km) where the NO_2 number density is relatively small compared to values at the peak altitude (25–30 km), this retrieval error is on the order of the correction due to the gradient effect (i.e. the relative difference between the 1-D and 2-D retrieval). The magnitude of these two quantities, i.e. the retrieval error (determined from the a-priori settings and the SCD retrieval error, Kühl et al., 2008, by the optimal estimation method, Rodgers, 2000) and the difference between the 1-D and 2-D retrieval are compared in Figs. 4 and 5 (in the middle and bottom panels): areas for which the retrieval error is larger than the difference between the 1-D and 2-D retrieval are shaded to distinguish them from those areas where the correction for the gradient effect is significant. It can be seen that for regions near e.g. the southern subtropics (10–30° S) or the southern part of the southern midlatitudes (around 60° S in Fig. 4) or the northern midlatitudes (around 40–60° N in Fig. 5) the gradient effect is larger than the retrieval error. For both orbits, differences between the 1-D and 2-D retrieval are around 10% just below the peak (approx. 30 to 25 km for the tropics and below 20 to 25 km for midlatitudes) and increase up to 30 or even 40% for altitudes around 20 km. Although rather similar absolute values of the effect appear at midlatitudes of both hemispheres, the relative effect is larger at the northern polar vortex boundary

because of lower NO_2 number density (see the values at 50–60° N in Fig. 5, bottom panel).

Comparing the results for the individual orbits with those of the mean of all full limb orbits (see Fig. 6), it appears that the differences between 1-D and 2-D retrieval are systematic and the regions where the difference is larger than the retrieval error mainly appear at the locations of the stratospheric transport barriers (compare Randel et al., 1993). Also for the mean, an increase of up to 2×10^8 molec./cm^3 for the 2-D retrieval with respect to 1-D retrieval can be seen at the southern part of the tropics and the southern part of the midlatitudes for altitudes that are below 20 to 25 km. This corresponds to 10–20% of the number density at the profile peak or ∼40% of the actual values. Also, a smaller increase at the midlatitudes of the Northern Hemisphere ($\sim0.5\times10^8$ molec./cm^3) is observed, which is up to 10% of the NO_2 number density at the profile peak. Compared to the differences found for individual orbits, smaller differences are found for the mean because of (1) the improved statistics because statistical retrieval errors of single orbits are (partly) averaged out and (2) averaging the longitudinal variability of the stratospheric transport barriers. This variability can be seen comparing the results for different orbits (compare Figs. 4 and 5), where for orbit 35499 the largest gradient at the subtropics occurs at 10-15°S but for orbit 35503 at ∼18° S. For the northern midlatitudes (40–60° N) the variation is even larger, showing a strong gradient for orbit 35503 but almost no gradient for orbit 35499.

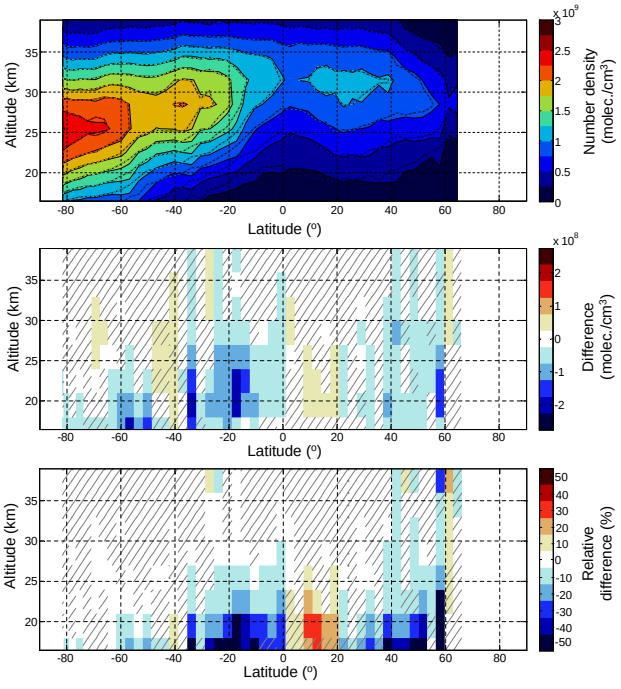

Fig. 6. Top panel: vertical and latitudinal distribution of the mean NO_2 number density for all six full limb orbits on 14 December 2008 retrieved by the 2-D approach (color plot with solid contourlines) and the 1-D approach (dashed contourlines). Middle and bottom panels: absolute and relative difference between results from the 1-D and 2-D approach for the retrieval boxes. Boxes where the retrieval error is larger than the difference are shaded by a diagonal pattern.

3.2 Studying a possibility for extending the 2-D retrieval for the nominal SCIAMACHY orbit by an interpolation constraint

If the distance between consecutive limb scanning sequences is 7.5°, as for the nominal SCIAMACHY measurement mode, the sensitivity regions of the scanning sequences are not sufficiently overlapping. Therefore, a direct application of the 2-D approach for these measurements is not possible without causing systematic errors comparable with those by the 1-D approach. In Sect. 2.3 we proposed a possibility to overcome this problem by an interpolation approach. In the following we study if this approach can be applied to improve the profile retrieval in cases of strong gradients also for the nominal SCIAMACHY orbit.

The full limb mode orbits offer the opportunity to test the performance of this approach simply by skipping every second limb scanning sequence in the retrieval and thus obtaining a resolution of 6.7° which is close to the nominal operational mode of the SCIAMACHY measurements. The results obtained by the interpolation approach for this resolution can then be compared with the values of the 2-D retrieval applied on all scanning sequences.

The comparison for the retrieved number density fields is shown as difference to the 2-D approach in Fig. 7 for orbit 35499 when the interpolation approach is applied on the odd numbered scanning sequences. For even numbered scanning sequences, not shown in the figure, similar discrepancies are found. A slightly better agreement with the 2-D retrieval is obtained by the interpolation approach than by the 1-D approach. However, large differences still appear for regions where the gradient is not changing gradually but e.g. changes its sign during the distance of two consecutive limb scanning sequences (e.g. at 38° S in Fig. 4), as seen in the second and bottom panel in Fig. 7. Nevertheless, for areas with a gradual increase of the number density where large differences are found for 1-D retrieval, more correct number densities with respect to the 2-D approach are retrieved by the interpolation approach (e.g. at 10°–20° S and 55° S or 20°–30° N, compare upper panel with the second panel from top). Also, for the mean of the retrieval of all full limb orbits, a better agreement with the 2-D retrieval can be seen for the interpolation approach than for the 1-D retrieval in the two bottom panels. However, the differences to the 2-D retrieval are in average only ∼25% smaller than for the 1-D retrieval for all limb orbits. Thus, only a small fraction of the gradient effect can be corrected.

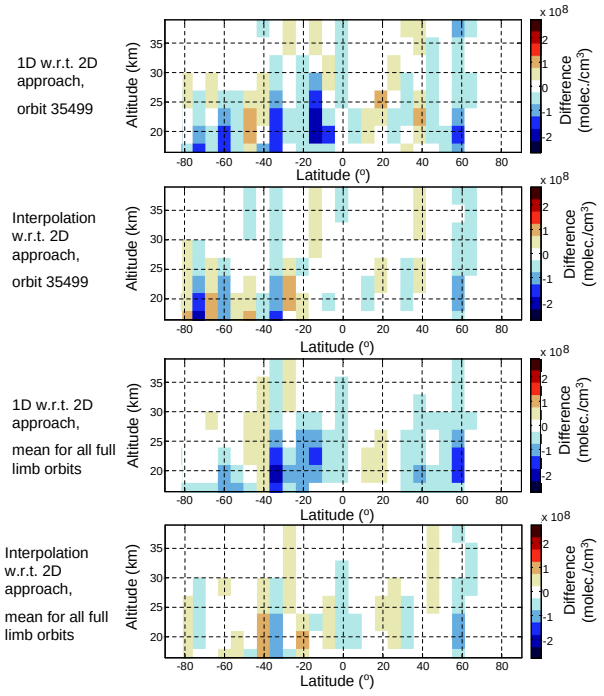

Fig. 7. Differences between the 1-D and 2-D retrieval (plotted for even scanning sequences) are shown in the first and third panel from top in comparison with the differences between the retrieval with interpolation approach (applied for even scanning sequences) and the 2-D retrieval (second and bottom panel). The first two panels show the differences for a single orbit (34599), the remaining panels the differences for the mean of all full limb orbits.

The possibility to improve the retrieval by the interpolation approach is studied here for the actual SCIAMACHY full limb orbits measured by SCIAMACHY, in Sect. 4 it is also verified by sensitivity studies on simulated data.

3.3 Impact of the gradient strength in the NO_2 distribution on the retrieved NO_2 profiles

In the following, we systematically investigate the relation between the steepness of the NO_2 gradient and its effect on the profile retrieval, i.e. the difference between the results acquired by the 1-D and 2-D approach. We study the gradient effect for the retrieved number densities at different altitudes (16–40 km) as well as for the stratospheric columns of NO_2 for all full limb orbits and all latitudes. The gradient strength G (for every horizontal altitude layer) is determined from the 2-D retrieval by calculating the difference of the retrieved number density n for a particular latitude region i to the previous latitude region $i-1$ along the LOS towards the instrument (i.e. northward), normalized by the distance d (in terms of degrees of orbital cycle) between these two measurements:

$$G = \frac{n_{i-1} - n_i}{d} \quad (5)$$

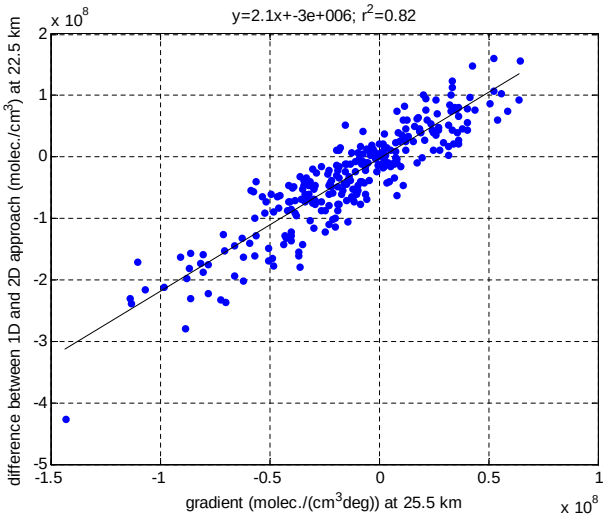

Fig. 8. Difference between the number density retrieved by the 1-D and 2-D approaches at 22.5 km as function of the horizontal gradient of the number density at 25.5 km as observed for the 2-D retrieval for all measurements of the full limb orbits on 14 December 2008. Also shown is the line of the best fit to the observed differences. Equation for the line of the best fit and squared correlation coefficient r^2 are provided in the title.

With this definition, the gradient is positive when the number density along the LOS towards the instrument increases and negative when it decreases.

Figure 8 shows the difference of the number density retrieved by the 1-D and the 2-D retrievals at 22.5 km altitude as function of the gradient at 25.5 km altitude for all full limb orbits. A clear linear dependency (squared correlation coefficient r^2=0.82) on the steepness of the gradient is found: a gradient in the number density of 10^8 molec./cm^3 per degree of the orbital circle of the satellite results in a difference of the number density of 2.1×10^8 molec./cm^3 (for the later scanning sequence) between both approaches.

To illustrate this effect also for other altitudes, Fig. 9 (left panel) shows the squared correlation coefficients (r^2) between the gradient strength and the difference between both approaches as a function of the gradient altitude (y-axis) and the altitude of the difference (x-axis). The strongest correlation is found for altitudes that are immediately below (i.e. $\sim$3 km) the altitude of the gradient. This is expected because the LOS crosses the number density field of the previous scanning sequence (for which the gradients are calculated) at higher altitudes before reaching the tangent point of the measurement (compare Fig. 2). The largest correlation (squared correlation coefficient $r^2>0.8$) occurs for gradient altitudes where the profile usually peaks (25–33 km), since here the effect from other altitudes and also the relative retrieval error is smaller. On the other hand, when the difference between the altitude of the gradient and that of the

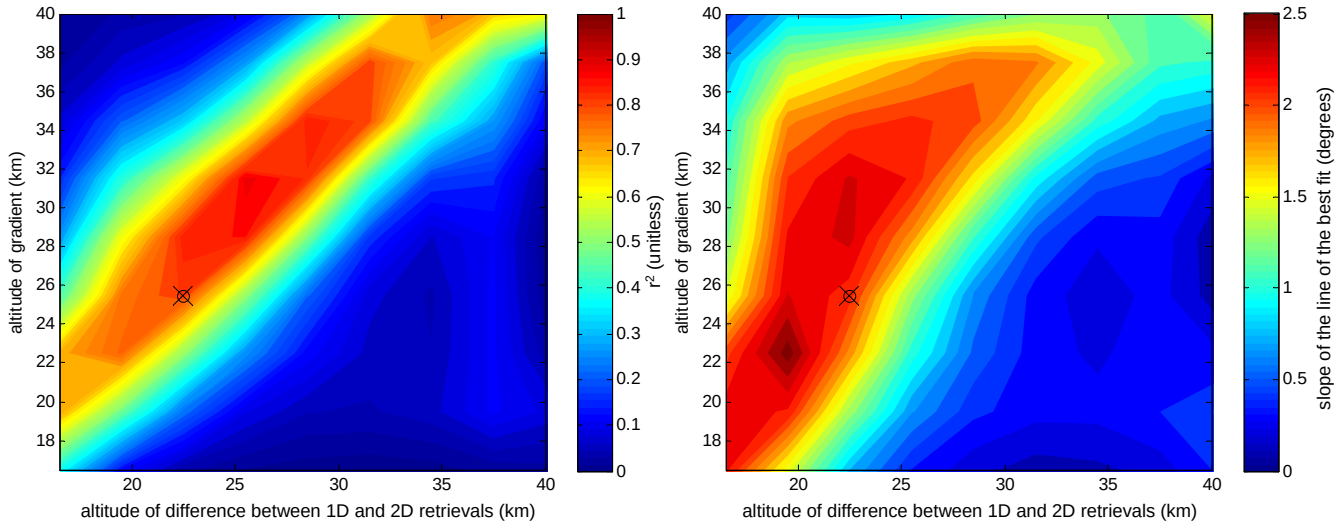

Fig. 9. Left: squared correlation coefficient (r^2) between gradients (calculated by Eq. 4) occurring at different altitudes and the difference between the 1-D and 2-D retrieval. Right: same as before but now the slope of the line of the best fit is shown. Values for the example plotted in Fig. 8 are indicated with a crossed circle.

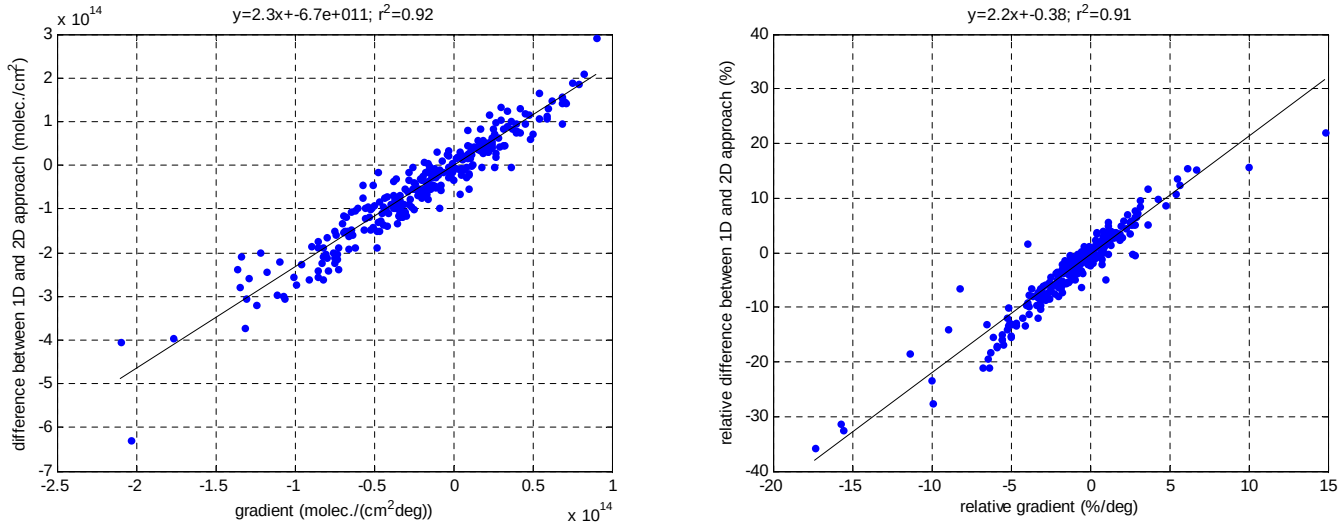

Fig. 10. Scatter plot between the gradient in the stratospheric NO_2 columns between 15 and 40 km as observed for the 2-D retrieval (between two consecutive scanning sequences) and the difference between the NO_2 columns retrieved by the 1-D and 2-D approach. On the left panel: scatter plots between absolute values, on the right: the same for relative values (normalized by the vertical column acquired by the 2-D retrieval). Also shown are the lines of the best fit to the observed differences. Equations for the lines of the best fit and squared correlation coefficients r^2 are provided in the titles.

number density to be retrieved increases, the correlation decreases. This can be explained by the fact that the length of the LOS that passes the field with the gradient decreases and therefore the retrieved number density is affected more by NO_2 number densities at altitudes that are closer to the particular altitude. Likewise, for differences that appear above the altitude of the gradient, the squared correlation coefficient is close to zero because the LOS does not cross the altitudes below. For cases with a large correlation, the value of the slope of the line of the best fit is in the range of 1.5–2.5 degrees for gradients below 38 km.

Since there is a strong effect of a gradient at a certain altitude for a wide altitude range below, the effect on the stratospheric NO_2 column is also significant. Fig. 10 (left panel) shows the scatter plot with the slope of the line of the best fit for the retrieved stratospheric column (integrated

from 15–42 km). A gradient in the vertical column of 1×10^{14} molec./cm^2 per degree of the Earth circle typically leads to a difference of $\sim2.3\times10^{14}$ molec./cm^2 between both approaches. Relative values for the analyzed orbits are indicated in the right panel of Fig. 10. It shows that most gradients for the stratospheric column are within an interval of $\pm5\%$ per degree of the orbital circle resulting in a difference of $\sim10\%$ in the obtained vertical column for the consecutive scanning sequence.

It should be noted that the retrieval is affected by statistical and systematical errors of the SCDs that further affect the retrieved number density profile. Since the difference and the gradient is calculated partly involving the same data (of the 2-D retrieval), the above study may partially be affected by these errors. However, as will be shown in Sect. 4 in sensitivity studies performed for simulated NO_2 distributions, similar correlations below the profile peak are found, also when the gradient is determined from the NO_2 distribution known before hand.

A possibility to reduce the effect of the retrieval error on the statistical relation between the gradient and the difference between the 1-D and the 2-D retrieval for the measured data would be to study in how far a gradient between some scanning sequences impacts those scanning sequences that are not involved in the gradient calculation. However, since the overlap in the sensitivity regions occurs only for two consecutive scanning sequences (as demonstrated later in the sensitivity studies), no trend is found if a correlation plot is made for the gradient between the first and second scanning sequence and the difference for the following third scanning sequence. Such an effect would be possible only if the measurements were performed on an even finer grid (distance between two limb scanning sequences smaller than 2°).

4 Studies on simulated data: verification and quantification of the profile retrieval correction by the 2-D approach

In this section we perform various sensitivity studies to investigate the effect of horizontal gradients in the NO_2 distribution on the profiles retrieved by the different 1-D and 2-D approaches. By applying the results of a model simulation from which the NO_2 distribution is well-known beforehand, the corresponding SCDs are calculated applying the RTM McArtim. Using these calculated NO_2 SCDs as input for the different retrieval approaches, the obtained profiles are then compared to the original (true) number density field. As NO_2 distribution field for the SCD simulation we apply first a simple linear gradient and later more realistic seasonal and latitudinal dependent NO_2 distributions obtained from the atmospheric chemistry model EMAC (Jöckel et al., 2006).

We also investigate the effect of the gradient strength on the systematic retrieval errors, i.e. the discrepancy between the retrieved and simulated (true) number densities and compare the results to those obtained by for the actual SCIAMACHY measurements. Further, studies on the estimation of the optimal distance between consecutive scanning sequences are performed.

4.1 Simulation of a linear gradient

For simulations of a simple scenario with a linear gradient, a stepwise gradient on a 20 times finer latitudinal grid than the measurement grid of the full limb orbits of SCIAMACHY is assumed for the SCD calculation. The profile is assumed to be of Gaussian shape with the peak at 28.5 km and a width of one standard deviation of 6 km (FWHM $\sim$14 km). The selected width approximately corresponds to the width of the NO_2 profile in the southern midlatitudes in December (determined from measurements and model data). We simulate different strengths of the linear gradient for which we calculate SCDs, that are later inverted by the 2-D or 1-D approaches, respectively.

In Fig. 11 an example for a case with a gradient from 5×10^8 molec./cm^3 at 50° N to 10×10^8 molec./cm^3 at 40° N (i.e. 0.5×10^8 molec./cm^3 per degree of the orbital circle in an interval of 10 degrees in latitude) at the profile peak is shown. The left plot in the upper row shows the number density field used for the calculation of the SCDs. The number density field interpolated on the SCIAMACHY measurement and retrieval grid is given on the upper right plot.

In the second row from top the number density field retrieved by the 1-D (on the left) and the 2-D approach (on the right) is shown. The third and bottom rows on the respective sides provide the absolute and relative differences to the interpolated simulation (true) field. Qualitatively, the results agree with the findings in Puķīte et al. (2008) showing a much better agreement with the true number densities for the 2-D approach than for the 1-D approach. For the latter, a significant disagreement especially for altitudes below the peak of the profile is observed. Quantitatively, the example in Fig. 11 shows that the gradient at the peak of 0.5×10^8 molec./cm^3 per degree of the orbital circle and the respective gradient for other altitudes (according to the Gaussian profile function) leads to a systematic retrieval error of around 1×10^8 molec./cm^3 for the 1-D retrieval for altitudes at 20 km. This corresponds to the findings in Sect. 3.3 where a very similar relation is observed (see Fig. 9, right panel), i.e. the gradient field at certain altitudes results in a discrepancy for the retrieval at altitudes below. For higher altitudes however, the number of altitude levels and thus the column of NO_2 above decrease, therefore the effect reduces. Thus, for the altitude of 25 km, just below the profile peak, the error is only 0.5×10^8 molec./cm^3, i.e. only half of the discrepancy below.

Due to the assumed linear gradient occurring at all altitudes, the scatter plots and slopes of the line of the best fit look different for the simulations (see Fig. 12) than for the real measurements (compare with Fig. 9). Since a similar

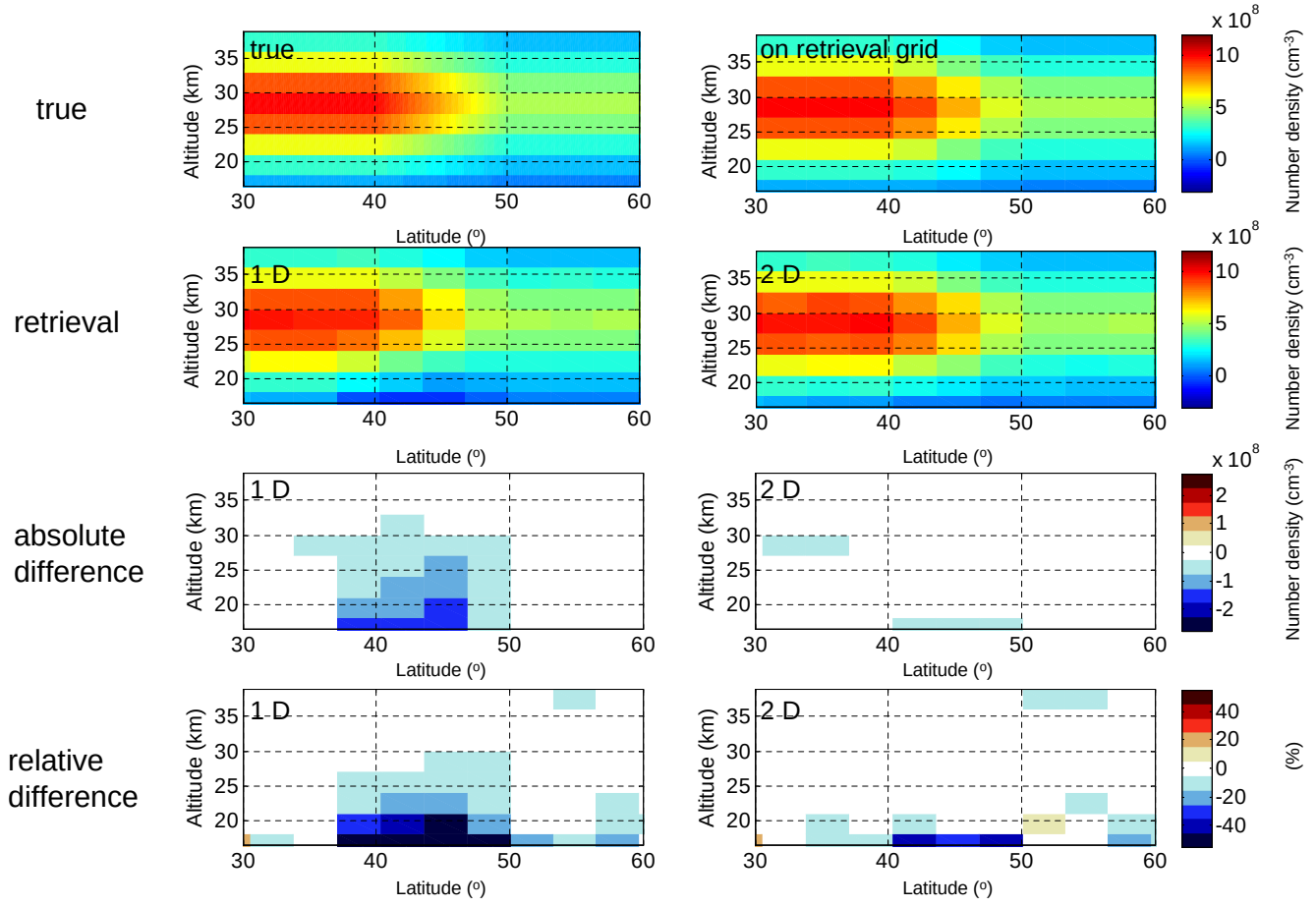

Fig. 11. Upper row left: assumed NO_2 distribution with a negative gradient towards the instrument. Upper row right: the same profiles but gridded on the SCIAMACHY retrieval grid. Second row: NO_2 profiles obtained by the 1-D retrieval (left) and 2-D retrieval (right). The absolute and relative differences between the original (true) profile averaged on the SCIAMACHY retrieval grid and the retrievals for the simulations are shown in the third and bottom row, respectively.

linear gradient with constant slopes at all altitudes is simulated, the gradient at any altitude causes the same correlation with the difference in number density at any particular altitude (see left panel). The correlation, however, is larger for differences below the profile peak because they are larger here and hence relatively less affected by the retrieval error. The slope of the line of the best fit (see right panel), however, is increased for altitudes above and below the profile peak because the differences are correlated with smaller gradients at these altitudes.

4.1.1 Latitudinal interval affected by the gradient

As seen in Fig. 11 (bottom row, left plot), the difference between the 1-D approach and the true NO_2 distribution is largest for latitudes around 42° N and 45° N. For the latitude region around 48° N an approximately two times lower discrepancy is observed, although the gradient occurs already at 50° N southwards. Similarly, lower discrepancies are obtained also around 39° N, where the gradient occurs only until 40° N. No effect can be seen northward from 50° N and southwards of 37° N. This shows that the gradient effect is limited to the latitudinal interval, where the gradient occurs and the next interval in the viewing direction of the instrument, not exceeding ∼3.5°. This small latitudinal interval for the gradient effect supports that we found no correlation for the real measurements between the gradient of two scanning sequences and the difference between the 1-D and 2-D retrieval for the following (third) scanning sequence (see Sect. 3.3).

4.1.2 Investigating the difference of the 1-D and 2-D retrieval for different gradient strengths

In analogy to the correlation studies for the actual SCIAMACHY measurements (see Fig. 9), we now investigate the linear dependency between the gradient strength and its effect on the profile retrieval also for the simulations, i.e. the

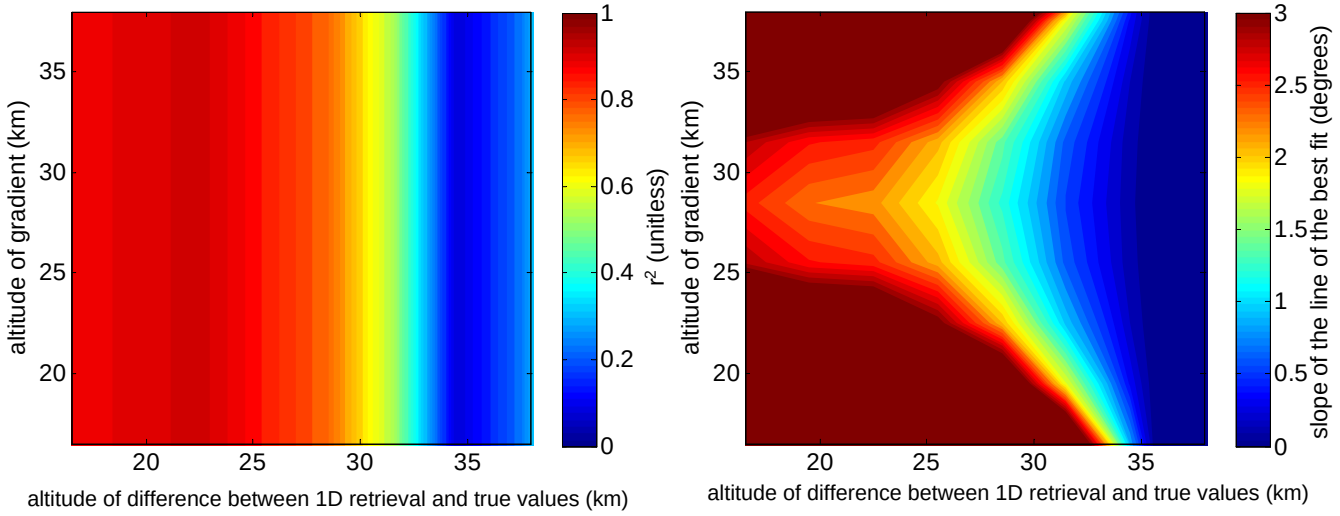

Fig. 12. Same as Fig. 9 but for the simulated linear gradient in Fig. 11. The differences are calculated between the 1-D retrieval and the true (simulated) data, the gradient is obtained from the true (simulated) data.

difference for the 1-D and 2-D approaches with respect to the simulated values as function of the gradient strength. Therefore we simulate SCDs for the simple Gaussian scenario with different gradient strengths by allowing the number density to increase more rapidly between 50° and 40° of latitude. In Fig. 13, the difference with respect to the true values is shown for the retrieved number density by the 1-D (left) and 2-D (right) approaches at 42° N for different altitudes and gradient strengths (on the x-axis, the gradient at the peak altitude, 28.5 km, is given). A clear linear dependency between the gradient strength and the related retrieval error is found. Also, the retrieval error increases for lower altitudes similarly as for the measurement. For the 1-D retrieval it varies between 1.5 and 3×10^8 molec./cm^3 for a gradient of 10^8 molec./cm^3 per degree of orbit cycle for altitudes from 25.5 to 16.5 km.

For the 2-D approach, a much better agreement with the true number density values is observed, although also here a linear increase of the discrepancy is found if the gradient strength increases. For the altitude of 16.5 km, the retrieval error is approx. 3.5 times smaller than for the 1-D approach. Nevertheless, the systematic disagreement (compare also Fig. 11) indicates that the distance of 3.3° may still be a bit too coarse as optimal distance for the tomographic approach, see also discussion in Sect. 4.1.3.

As a summary, the Fig. 13 verifies the finding of Sect. 3: neglecting the typical gradient of 0.5 to 1×10^8 molec./cm^3 per degree of the orbital circle leads to errors in the retrieved number density of 0.5–3×10^8 molec./cm^3. Relative to the typical peak number densities of NO_2 this corresponds to 10 to 30%, but relative to the actual number density at a given altitude it can exceed even 50%. This is in agreement with the observed differences between the 1-D and 2-D retrieval for the measurements (Sect. 3.3), verifying that the additional retrieval error for the measurements only has a small impact on this systematic difference.

Note that due to the assumption of a linear gradient, similar studies for the interpolation approach would yield similar results as for the 2-D approach because the gradient would be fitted by the linear interpolation.

4.1.3 Impact of the distance between consecutive scanning sequences on the 2-D retrieval

As shown before, the 2-D approach for the full limb orbits with a distance between the consecutive scanning sequences of ∼3.3° improves the retrieval considerably with respect to the 1-D approach. In the following we study the effect of different spacings for the tomographic retrieval.

For this study, additionally to the distance of 3.3°, we simulated SCDs for the scanning sequences performed with a two times coarser and a two times finer resolution. It is worth to remind that the two times coarser resolution (6.7°) nearly fits with the resolution for the nominal orbits (∼7.5°). We simulated SCDs for the same gradient settings (0.5×10^8 molec./cm^3 per degree of orbital cycle at the peak of the profile) as in Sect. 4.1 but with the gradient extending from 50° up to 35° N (see top graph on the left panel in Fig. 14) in order to assure that for the simulation with the coarser resolution the gradient occurs for two scanning sequences.

The retrieved number density distributions are compared with the true distributions and are shown on the left panel in Fig. 14.

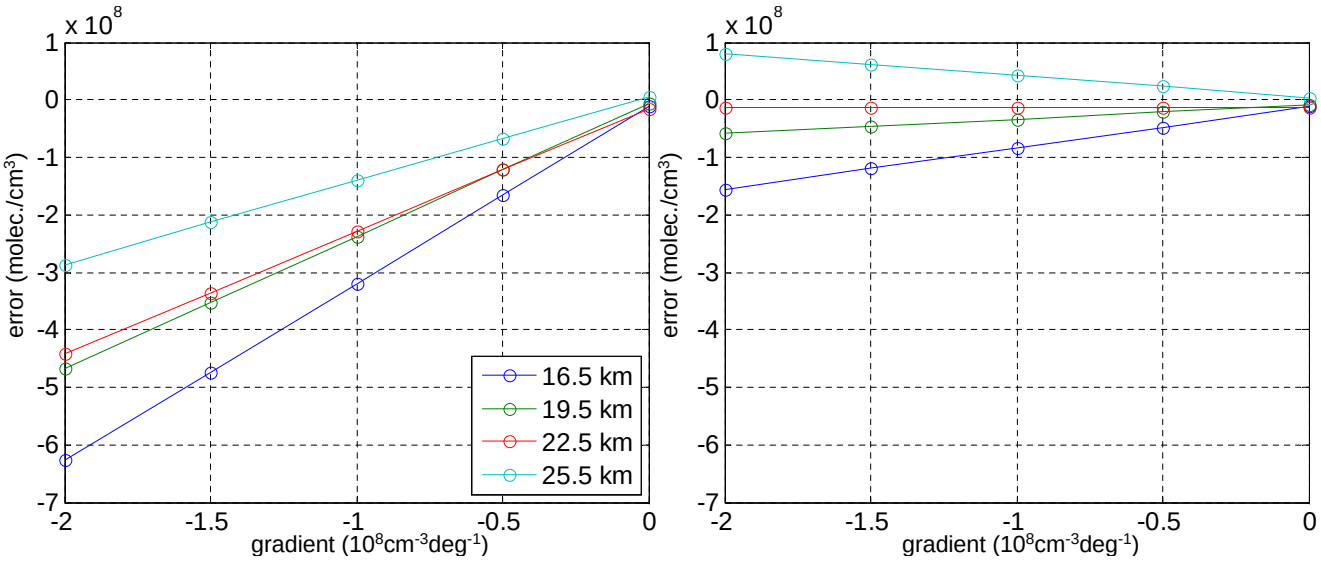

Fig. 13. The systematic error at 42° N in the retrieved number density of NO_2 as function of the simulated gradient strength between 40° and 50° for the 1-D (left) and 2-D (right) retrieval approach. On the x-axis the gradient strength at the peak of the simulated profile (28.5 km) is given. The colored lines display the difference to the true simulated values at the respective altitudes (16.5 km to 25.5 km, see legend).

For the cases with a spacing of 3.3° and 1.7°, only small discrepancies to the true values are found for the gradient region with the exception of a slight underestimation (up to 0.4×10^8 molec./cm^3) for the case of 3.3° at 16.5 km. This overall good agreement is also observed for the southern part of the gradient area (approx. 38 to 42°), where the TP and the LOS are within the gradient region and therefore the measurement is strongly sensitive to the gradient. For this area, the average difference between the 2-D retrievals performed for the different spacings and the true distribution is plotted in the right panel of Fig. 14. Thus, without considering the argument that any additional sampling is improving the statistics of the measurement, it can be concluded that a distance in the interval between 3.3° and 1.7° (i.e. ∼3°) allows to correct for the horizontal gradient effect and thus is successfully reducing the systematic error towards the retrieval noise for the gradient of 0.5×10^8 molec./cm^3 per degree of orbital cycle. However, as can be seen for the case with a distance of 1.7°, further reducing the distance also increases the retrieval noise, thus showing limited improvement for this gradient strength w.r.t. the distance of 3.3° (although it improves the overlapping of consecutive scanning sequences and corrects well for the systematic discrepancies). For very small distances, like 1.7 deg, a smoothing constraint could be introduced to reduce this noise, but then the retrieval resolution will be downgraded.

Much larger discrepancies are found for the case with the coarse resolution of 6.7° (second plot from top). This is observed for latitudes affected by the gradient and also for the first latitude region after the cease of the gradient. At the peak of the profile, the error is up to $\sim1\times10^8$ molec./cm^3, and thus of the same magnitude as the errors found for the 1-D approach. This indicates that for such a coarse spacing the sensitivity regions do not overlap well enough to successfully apply the 2-D tomographic retrieval.

4.2 1-D and 2-D retrieval applied on simulations for EMAC NO_2 distributions

To investigate the effect of a gradient in the NO_2 distribution on the profile retrieval and the ability of the 2-D tomographic approach to correct for it also for more realistic cases, we apply NO_2 distributions calculated by the ECHAM/MESSy Atmospheric Chemistry EMAC general circulation model (Jöckel et al., 2006). To study the seasonal effect, we selected the distributions for the day 15 of March, June, September and December 2007. Note that model simulations for the year 2008 are not considered here because an actual quantitative comparison of the observed and simulated NO_2 data is not in the scope of this article. The model output is obtained at the local time of SCIAMACHY measurements for the illuminated part of the orbit within the latitudinal range between −80 and 80° with a horizontal resolution of 2.78° and a vertical resolution of 600–800 m in the stratosphere. The SCDs are calculated for the orbital geometry of SCIAMACHY limb measurements with a spacing between the consecutive scanning sequences corresponding either to the nominal or the full limb operational mode (7.5° or 3.3° of the orbital circle). For the simulations in our studies the NO_2 number densities are gridded on a 40 times finer latitudinal grid than that of the scanning sequences in the nominal

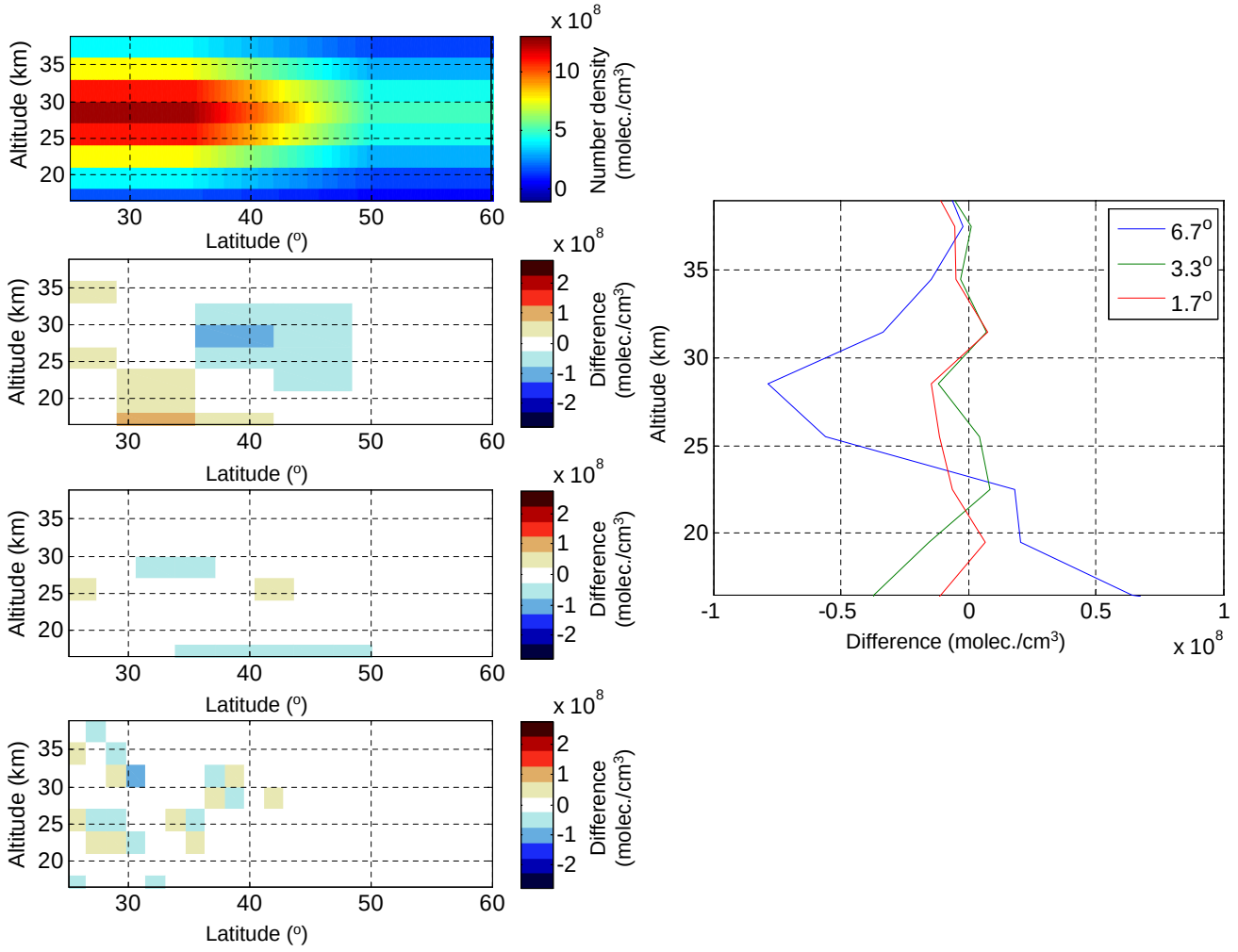

Fig. 14. 2-D retrieval for different distances between consecutive scanning sequences. On the left: the NO_2 field of the simulation (top) and the differences between the retrieved number density and the true values with the distance of 6.7° (second plot), 3.3° (third plot) and 1.7° (bottom plot). On the right: mean differences are plotted for the southern part of the gradient (i.e. where the measurement is sensitive only to the areas of the gradient) for the three distances.

SCIAMACHY operational mode (i.e. 7.5°/40) in order to allow a smooth latitudinal change in the number density in the RTM. Also, we grid the data on a 3 km altitude resolution, thus matching the vertical retrieval grid.

In Fig. 15, the simulated NO_2 number density field (upper plot, left panel) for 15 December 2007 is provided. The second plot (left panel) shows the number density field (gridded) as it is applied for the calculation of the SCDs. The number density field interpolated on the nominal SCIAMACHY measurement and retrieval grid (corresponding to the spacing of scanning sequences of 7.5° of the orbital cycle) is given in the third plot. The same, corresponding to the full limb mode with horizontal spacing of 3.3° is shown in the bottom plot.

The figure also shows the absolute and relative differences between the retrieval methods and the simulated (true) number density field (middle and right panel). It can be seen that the 1-D approach (top panels) shows significant discrepancies (around 1 to 2×10^8 molec./cm^3) for the latitudes where the strong gradients occur (around 20° S and 20° N at the subtropics, arround 60° S and 40–60° N). At these latitudes the gradients reach 0.5 to 1×10^8 molec./cm^3 per degree. The regions and also the magnitude of the differences agree well with the results obtained for the real measurements for the mean of the full limb orbits in Fig. 6.

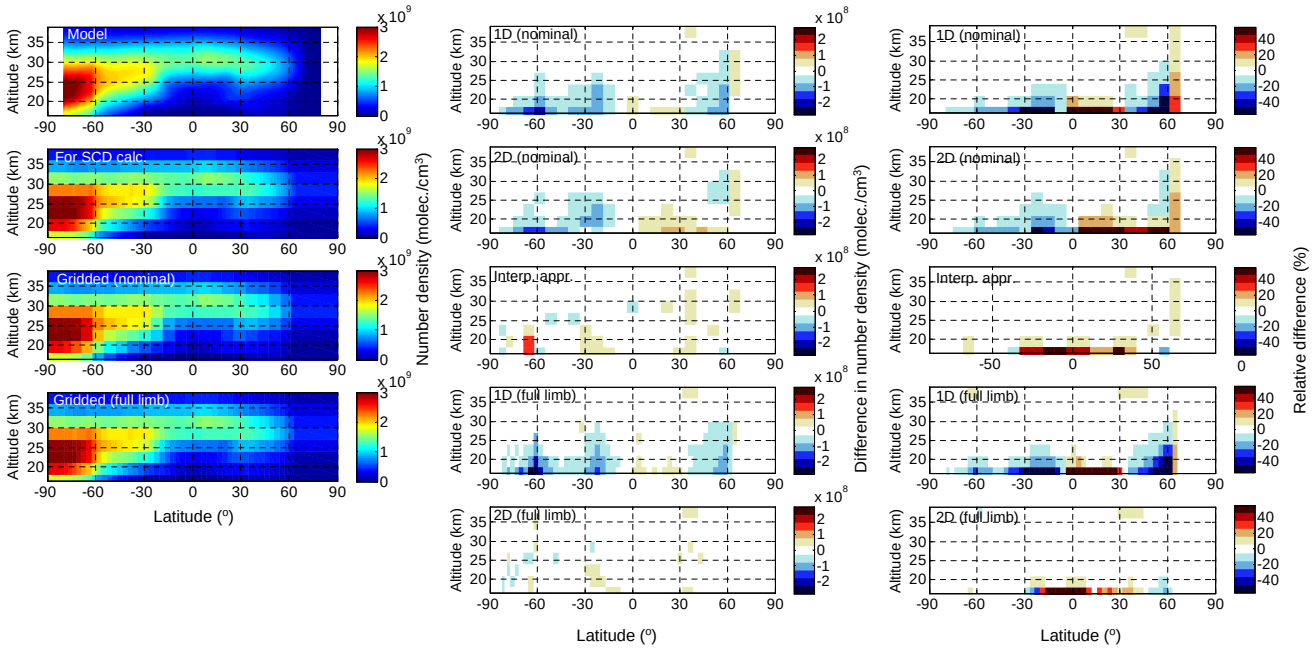

Fig. 15. Left panels: NO_2 number density field simulated by EMAC atmospheric chemistry general circulation model for 15 December 2007 (top), gridded for the simulation of SCDs with fine horizontal resolution (second row), and gridded to the resolution of the SCIAMACHY limb measurements in the nominal and full limb operational modes (third and bottom row). In the middle and right panels absolute and relative differences between the NO_2 distribution retrieved from the simulated SCDs and the true (simulated) number density field are shown. The first three rows from top show results for the simulated measurements with the distance of 7.5° of the orbital cycle between consecutive scanning sequences. From top to bottom the differences plotted are for the 1-D approach, the 2-D approach and the interpolation approach. In the two bottom rows, the results for the distance of 3.3° (i.e. full limb mode) are shown for the 1-D and 2-D approach.

4.2.1 Influence of the spacing between scanning sequences on the 2-D retrieval and investigation of the interpolation approach

In Fig. 15 it can also be seen that when applying the 2-D approach to the simulations for the nominal SCIAMACHY mode, with a spacing of 7.5° of the orbital cycle, the retrieval can not be improved by the 2-D approach (second panel from top) and has similar discrepancies as the 1-D approach. For this distance the sensitivity areas of the consecutive scanning sequences are not overlapping and therefore the 2-D approach does not provide additional information.

On the other side, for this spacing an improvement can be acquired by applying the interpolation approach (third panels from top in Fig. 15). It should be noted that such a good agreement may, however, not be obtained, if the gradient is not so smooth and varies significantly within sensitivity areas of limb measurements and between scanning sequences because the coarser sampling cannot resolve the finer variations this is not occurring in the simulated example because of the limited horizontal resolution or is affected by the measurement error.

The 2-D approach applied on the simulations with a spacing between the consecutive scanning sequences of 3.3° (bottom panels), i.e. like for the full limb orbits, significantly improves the agreement with the simulated field. The systematic errors for the 1-D approach at around 25° or 60° S and also at 50° N are corrected by the 2-D retrieval. The remaining errors are on the level of the retrieval noise. Thus, a retrieval with an even finer resolution will not provide significant additional improvement (compare with Sect 4.1.3). It should however be noted, that, in general, with an increased resolution, i.e. by a closer spacing, more information can be gained from the measurements. Therefore the 2-D retrieval with the small spacing is more accurate compared to the interpolation approach with a two times larger spacing for the cases with rapid changes in the atmospheric number density (compare e.g. the difference at 20–30° S or around 60° S).

The study is performed also for other months for which the gradients at the locations of the transport barriers (i.e. at subtropics and between midlatitudes and polar regions) are also very pronounced (see Appendix A). Therefore the discrepancies for the 1-D (and also the 2-D approach with nominal spacing) appear mainly for these regions. Also for these months the largest improvement is obtained with a spacing between the consecutive scanning sequences of 3.3°.

4.2.2 Effect of the gradient on the systematic retrieval error

Similarly as for the measured data, we performed statistical studies regarding the effect of the gradient at different altitudes on the systematical retrieval error of the 1-D retrieval: in Fig. 16 the squared correlation coefficients (left panel) and the slope of the line of the best fit for the relation between the gradient and the difference between the 1-D retrieval and the simulated field (right panel) are given.

Like for the measurement results in Fig. 9, the correlation is large only for altitudes below the altitude of the gradient. The squared correlation coefficient r^2 is up to 0.7 for these altitudes. The slope of the line of the best fit is around 2 degrees for these altitudes, i.e. a gradient in the number density of 1×10^8 molec./cm^3 per degree of the Earth circle leads to an error of 2×10^8 molec./cm^3 for the 1-D approach. This finding is in good agreement with the slope obtained for the measurements plotted in Fig. 9.

The large values of the slope of the line of the best fit for the gradients at high altitudes may not be explained by the gradient effect because of the small squared correlation coefficient for these cases. Note that the larger values of the squared correlation coefficient for the real measurements (in comparison to the simulations) arise due to a different calculation of the gradient: for the simulations, the gradient is calculated from the (true) distribution known before hand; for the measurements, it is calculated from the distribution retrieved by the 2-D approach. Also the difference is obtained w.r.t. the distribution known before hand for the simulated data but w.r.t. the distribution retrieved by the 2-D approach for the measurements. Therefore, statistical and systematical retrieval errors may contribute to the determined gradient strength. On the other hand, a lower correlation for the simulated data can also appear because the gradient may be different at different latitudes also in between the TPs of the simulated measurements, but for the calculation of the gradient only the concentration values at the TPs are applied.

In analogy to Figs. 8 and 10, Fig. 17 shows the scatter plot of the gradient at 25.5 km and the difference at 22.5 km (left panel), together with the relation between the gradient of the stratospheric column and its impact on the retrieval (right panel). Again, a linear dependency is observed (with a squared correlation coefficient of r^2=0.59 for the number density and 0.8 for the stratospheric column density). Compared with the results for the measurements, there is a good agreement regarding the amplitude of the gradient which ranges from approx. 0.3 to -0.5×10^8 molec./cm^3 (number density at 25.5 km) for the bulk of both datasets. Also, for the gradient of the integrated stratospheric column density, comparable values are found, ranging from 0.2 to -1×10^8 for the simulations and 0.6 to -1.4×10^8 molec./cm^2 for the measurements (see Fig. 10, left panel). The smaller amplitude of the gradient in the model data compared with the measured gradient may be explained by the limited resolution in the model and the fact that the model data is a zonal average. Also note that in contrast to the measurement results in Figs. 8 and 10, the differences and the gradients are calculated with respect to the true NO_2 distribution field. The smaller correlation (which means more outliers) may affect the slope of the line of the best fit which is 1.4 (number density for the example altitude) and 1.9° (stratospheric column density) for the simulation compared with 2.1° and 2.3° for the measurement. Considering these points, the results for the simulations and the measured data both show a very similar effect of an existing gradient on the 1-D retrieval.

5 Conclusions

The tomographic 2-D approach for the retrieval of vertical profiles from the SCIAMACHY limb measurements (Puķīte et al., 2008) was applied for the full limb orbits performed on 14 December 2008. We show that the method improves the retrieval for altitudes at and below the profile peak with respect to the 1-D approach by ∼10 to 20% of the peak value (or up to 50% of the actual value) of the NO_2 number density. The difference is largest at subtropics and between southern mid-latitudes and polar regions in December where a gradient of 0.5 to 1×10^8 molec./cm^3 per degree of the orbital cycle is observed below 25 km due to the stratospheric transport barriers.

In the sensitivity studies we verified the discrepancies introduced in the profile retrieval if the horizontal gradient is not considered. First, we performed simulations by assuming a simple linear gradient and second, by applying NO_2 distributions from the EMAC atmospheric chemistry general circulation model. The simulations with the modelled data provided similar discrepancies between the 1-D retrieval and the simulated data like the observed discrepancies between the 1-D and 2-D retrieval for the measured data. In both datasets, linear dependency between the horizontal gradient strength and the systematic retrieval error for the 1-D retrieval is found. In contrast, the tomographic 2-D retrieval shows only very small discrepancies in comparison to the true NO_2 distribution. Thus, for reducing the systematic retrieval error, the 2-D retrieval is more important the stronger the horizontal gradients of the retrieved trace gas are.

The sensitivity studies for the full limb orbits also revealed that a certain gradient affects only the retrieval at the scanning sequence for which the tangent point lies within the gradient region and the scanning sequence immediately after this interval. Thus, the length of the impact of the gradient does not exceed the distance between the scanning sequences (i.e. 3.3° of the orbital cycle). We also found that a linear gradient can almost completely be accounted for by the 2-D approach for such a resolution and show that a further decrease of the distance between the consecutive scanning sequences provides only a negligible improvement. Also, the studies on seasonal NO_2 data from EMAC show that the gradient is

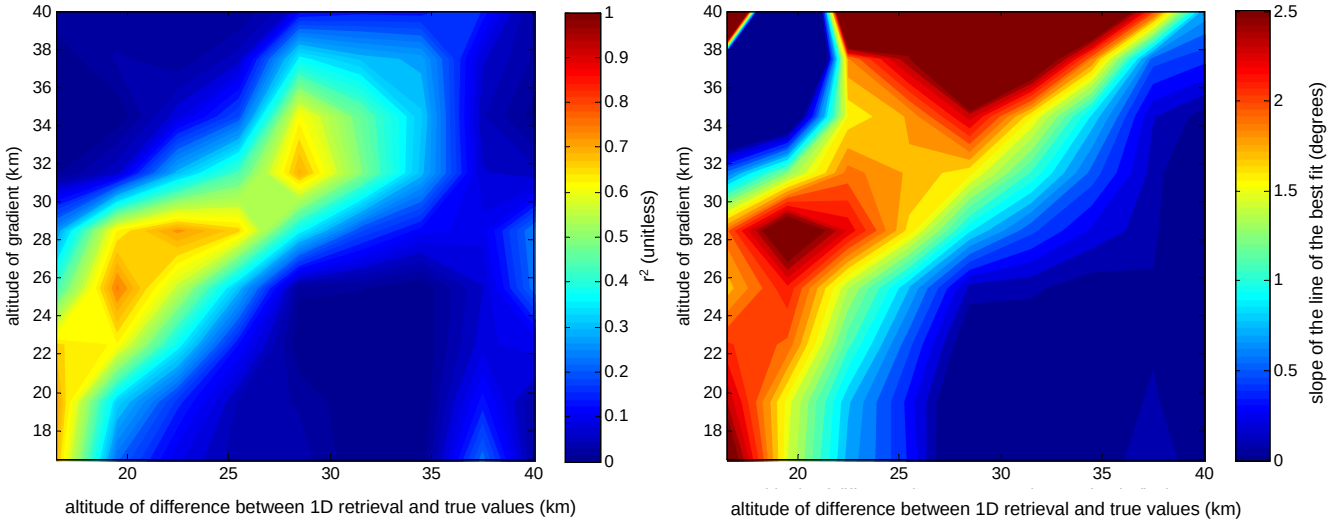

Fig. 16. Same as Fig. 9 but for simulated data for 15 December 2007. The differences are calculated between the 1-D and true (simulated) data, the gradient is obtained from the true (simulated) data.

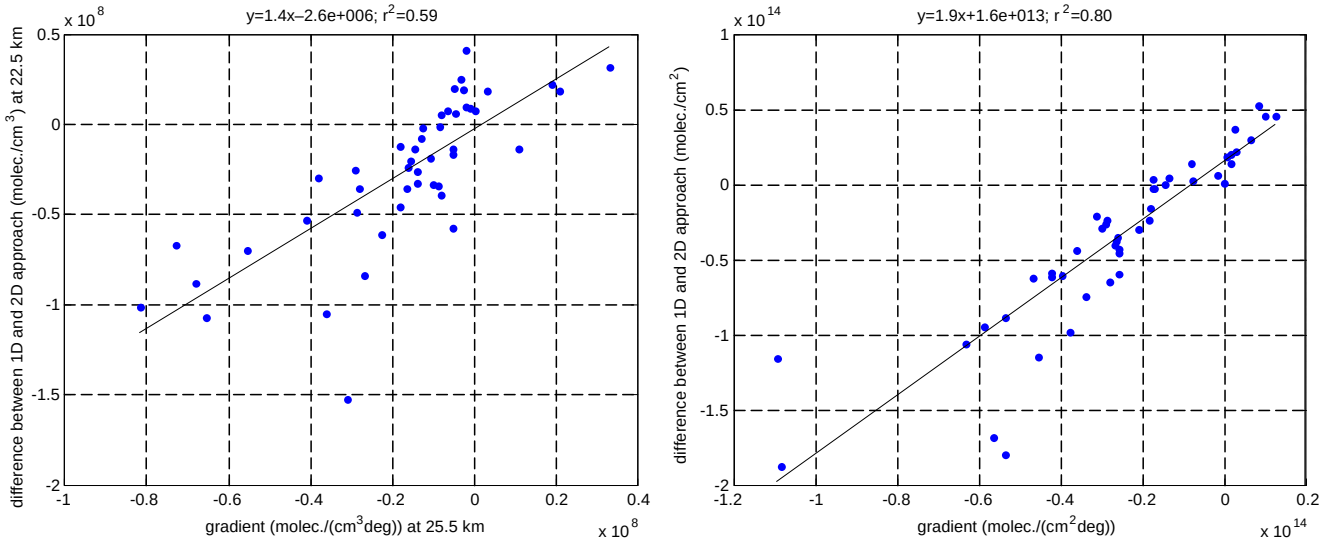

Fig. 17. Left panel: difference between the number density retrieved by the 1-D approach and the true data at 22.5 km as function of horizontal gradient in the number density at 25.5 km for 15 December 2007. Right panel: same, but for the stratospheric column between 15 and 39 km. Also shown is the line of the best fit to the observed differences. Equations for the lines of the best fit and squared correlation coefficients r^2 are provided in the titles.

well accounted for with such a distance. On the other hand, no improvement is obtained when the 2-D approach is applied for coarser distances between the scanning sequences: for the distance of 7.5° (corresponding to the nominal operational mode of SCIAMACHY), the 2-D approach results in similar discrepancies to the true distribution as the 1-D approach.

The possibility to apply an interpolation approach, assuming a linear gradient in between the locations of the actual measurement, was investigated. We applied the interpolation approach for full limb orbits skipping every second scanning sequence in the retrieval thus obtaining a spacing between the measurements that is comparable with that of the nominal SCIAMACHY orbits. The results allow us to conclude that although no overlap of the sensitivity areas for

the measurements in the nominal SCIAMACHY operational mode exists, the interpolation approach agrees better with the 2-D retrieval than the 1-D approach for all full limb mode scanning sequences. However, only a small part of the gradient effect can be corrected for by this approach. In case studies we find that the 1-D retrieval shows up to 25% higher discrepancies with respect to the 2-D retrieval (applied for all scanning sequences) than the retrieval with the interpolation approach (applied for every second scanning sequence of the full limb orbit).

Based on the findings for the full limb orbits, the retrieval for the nominal orbits should be modified to limit the horizontal gradient effect. Different approaches might be considered. Besides the interpolation approach, also an empirical correction for the 1-D retrieval could be performed, taking into account the gradient between the retrieved profiles of the consecutive scanning sequences. As well, gradients provided by atmospheric chemistry models may be used for the correction. Also, the assimilation of profiles retrieved from SCIAMACHY for the previous days can be considered. In upcoming studies it will also be investigated in how far nadir measurements might be involved in a tomographic approach. Although nadir observations provide information on the total column only, they could provide more detailed information on the location of the gradient in the horizontal dimension.

The current study shows that SCIAMACHY is able to perform limb measurements for which a global tomographic approach can be implemented that provides NO_2 profiles with a discrepancy to the true distributions on the level of the measurement noise. Up to present these full limb measurements are limited to a few orbits on 14 December 2008. Due to the large systematic errors, for the 1-D retrieval approaches, in particular for regions close to stratospheric transport barriers, the interpretation of these data in scientific studies is limited. In this article, the impact of horizontal gradients was investigated for the retrieval of NO_2. However, similar retrieval errors can also be expected for other trace gases if comparable horizontal gradients occur. Therefore, it may be useful to extend the full limb measurements for selected events of particular interest and/or on a routine basis for different seasons to establish a climatology of 2-D profiles. The smaller systematic errors of the 2-D retrieval might also be useful when the limb-nadir matching is performed for the determination of tropospheric nadir columns (Beirle et al., 2010).

Appendix A

Simulation of the gradient for different seasons

Additionally to the simulation for the EMAC distribution of NO_2 for 15 December 2007 in Sect. 4.2, we perform the study also for three other days representing different seasons. We simulate SCDs and retrieve NO_2 distribution fields for 15 of March, June and September (Figs. A1, A2, and A3). Also for these days and seasons the gradients are very pronounced at the locations of the transport barriers (i.e. at the subtropics and between midlatitudes and polar regions). While there are strong seasonal variations in the absolute values of NO_2 for the midlatitudes and polar regions, very similar number densities are observed for all seasons in the tropics. Therefore, the gradient strength and the resulting systematical errors in the 1-D retrieval are similar with those found for December in Fig. 15 for the tropics.

In March and September an almost symmetrical distribution of NO_2 is observed for midlatitudes in both hemispheres. Thus, only very small gradients are observed between midlatitudes and polar regions. For these months, the interpolation approach shows a better agreement with the true distributions approach in contrast to the results for December and June. The largest gradients take place at the subtropics where, besides the increase of the number densities towards midlatitudes, also the altitude of profile peak decreases.

In September (see Fig. A3), however, a very strong decrease of NO_2 occurs also within the Antarctic polar vortex and therefore much stronger gradients than usual appear (in the Fig. A3 between 60 and 75° S). It can be seen that even for such a strong gradient the interpolation approach and 2-D approach (with the spacing between the consecutive scanning sequences of 3.3°) retrieve number density values that are much closer to reality. The large relative differences for altitudes below 20 km for the most southern part of orbit (75–80° S) appear because these differences are caused by a gradient through areas with high NO_2 number densities outside and very low NO_2 values within the polar vortex.

In June, an increase in the NO_2 number density towards the Northpole occurs in contrast to December where it appears towards the Southpole. Therefore, strong positive gradients towards the instrument are observed in the Northern Hemisphere comparable with the negative gradients in the Southern Hemisphere in December. Thus, a strong overestimation for the 1-D retrieval occurs in the Northern Hemisphere at subtropics and midlatitudes, the strongest at 10° N and 60° N, i.e. at the transport barriers.

These case studies show that, although the strength of the horizontal gradient in NO_2 varies seasonally, the correction for it in the retrieval is important for every season. For all studied cases, the 2-D approach reduces the discrepancy to the true distributions up to the level of the measurement noise.

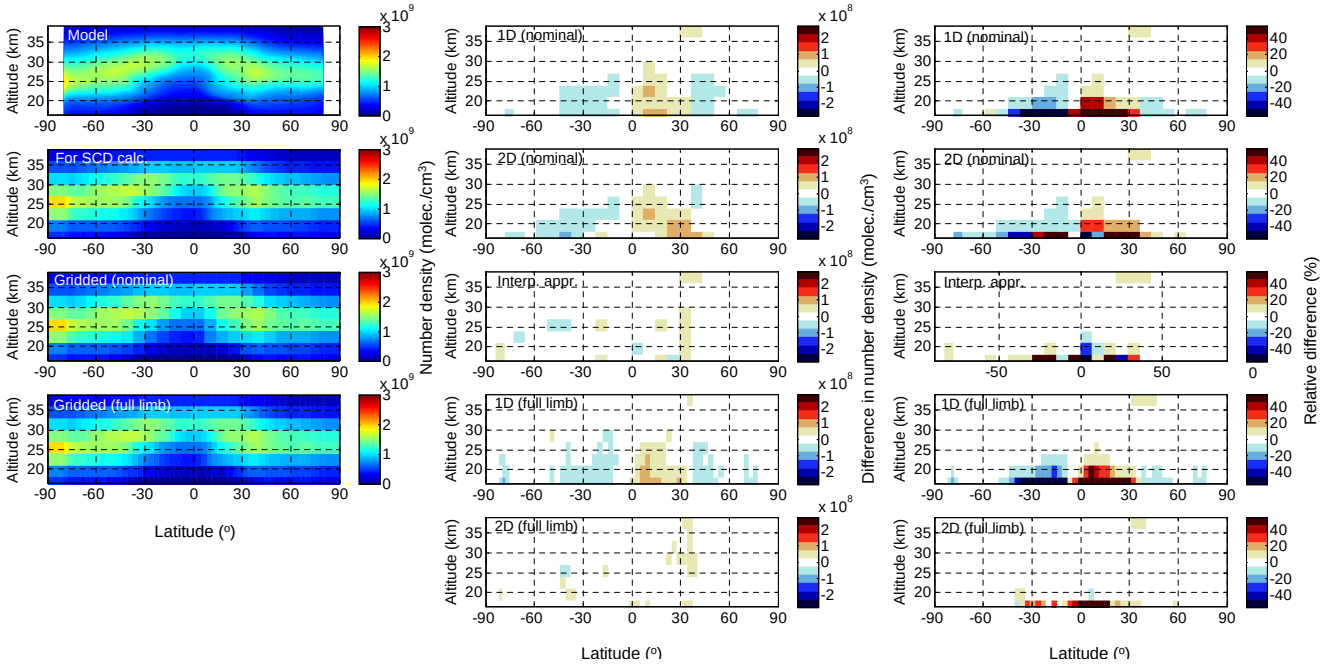

Fig. A1. Same as Fig. 15 but for 15 March 2007.

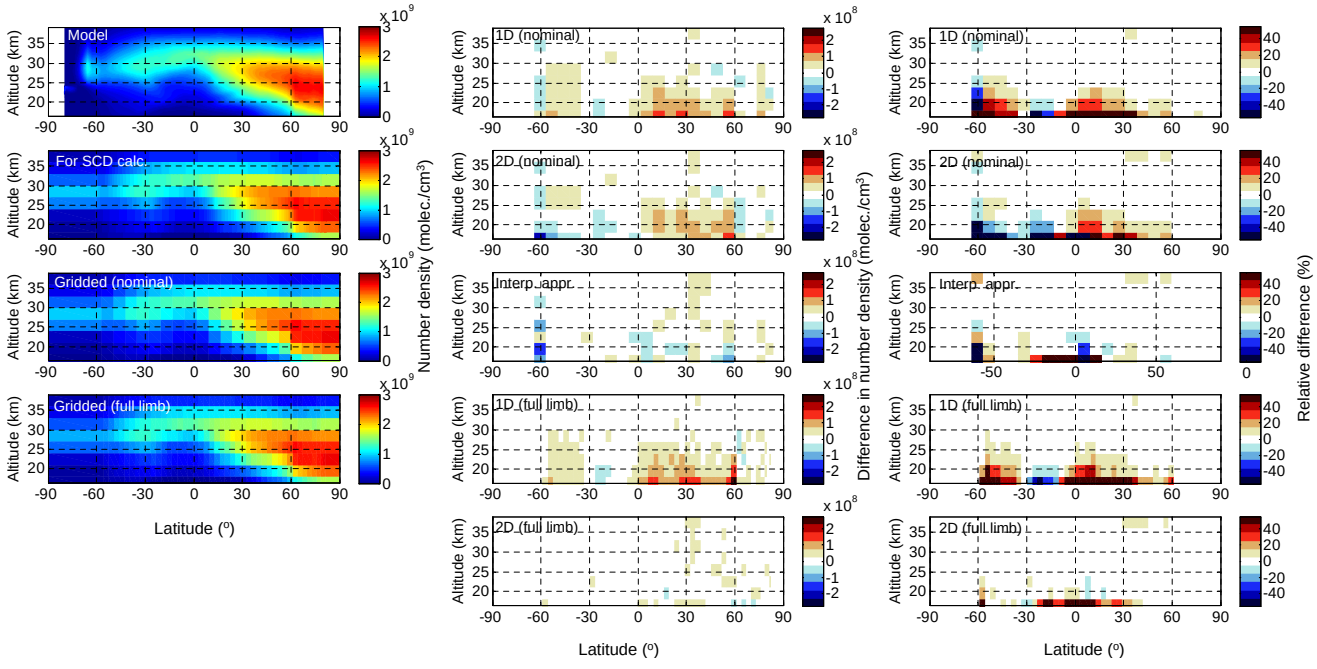

Fig. A2. Same as Fig. 15 but for 15 June 2007.

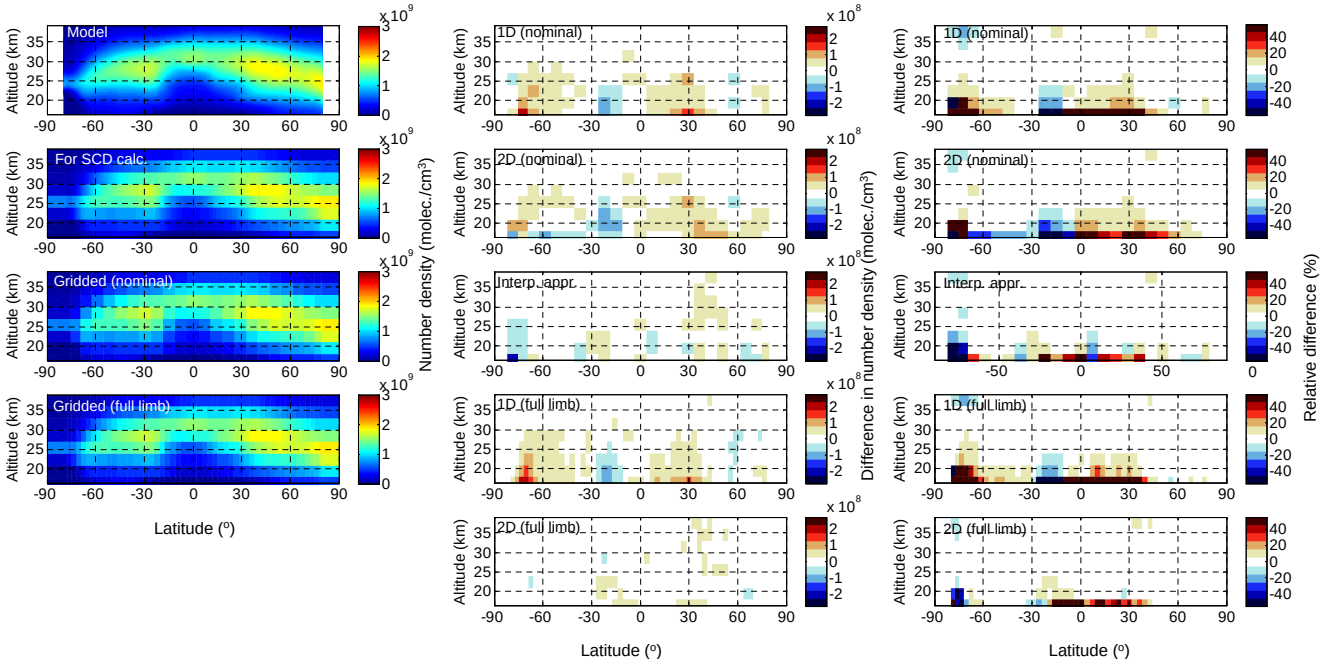

Fig. A3. Same as Fig. 15 but for 15 September 2007.

Acknowledgements. We want to thank ESA and DLR for providing the SCIAMACHY level 1 data and implementing the Operational change request no. 38 "Full limb mode orbits for assessing the horizontal gradient effects on profile retrieval". One author (S. Kühl) is funded by the DFG (Deutsche Forschungs Gemeinschaft).

The service charges for this open access publication have been covered by the Max Planck Society.

Edited by: C. von Savigny

References

Beirle, S., Kühl, S., Puķīte, J., and Wagner, T.: Retrieval of tropospheric column densities of NO_2 from combined SCIAMACHY nadir/limb measurements, Atmos. Meas. Tech., 3, 283–299, doi:10.5194/amt-3-283-2010, 2010.

Bovensmann, H., Burrows, J. P., Buchwitz, M., Frerick, J., Noël, S., Rozanov, V. V., Chance, K. V., and Goede, A. P. H.: SCIAMACHY: Mission objectives and measurement modes, J. Atmos. Sci., 56, 127–150, 1999.

Brasseur, G. P. and Solomon, S.: Aeronomy of the Middle Atmosphere, edited by: Brasseur, G. P. and Solomon, S., Kluwer Academic Pub., 644 pp., 2005.

Carlotti, M., Brizzi, G., Papandrea, E., Prevedelli, M., Ridolfi, M., Dinelli, B. M., and Magnani, L.: GMTR: Two-dimensional geo-fit multitarget retrieval model for Michelson Interferometer for Passive Atmospheric Sounding/Environmental Satellite observations, Appl. Optics, 45, 716–727, 2006.

Carlotti, M., Dinelli, B. M., Raspollini, P., and Ridolfi, M.: Geo-fit Approach to the Analysis of Limb-Scanning Satellite Measurements, Appl. Optics, 40, 1872–1885, 2001.

Degenstein, D. A., Llewellyn, E. J., and Lloyd, N. D.: Volume Emission Rate Tomography from a Satellite Platform, Appl. Optics, 42, 1441–1450, 2003.

Deutschmann, T.: Atmospheric radiative transfer modelling using Monte Carlo methods, Diploma thesis, Universität Heidelberg, Heidelberg, Germany, 2009.

Jöckel, P., Tost, H., Pozzer, A., Brühl, C., Buchholz, J., Ganzeveld, L., Hoor, P., Kerkweg, A., Lawrence, M. G., Sander, R., Steil, B., Stiller, G., Tanarhte, M., Taraborrelli, D., van Aardenne, J., and Lelieveld, J.: The atmospheric chemistry general circulation model ECHAM5/MESSy1: consistent simulation of ozone from the surface to the mesosphere, Atmos. Chem. Phys., 6, 5067–5104, doi:10.5194/acp-6-5067-2006, 2006.

Kühl, S.: Quantifying Stratospheric chlorine chemistry by the satellite spectrometers GOME and SCIAMACHY, Ph.D. thesis, Universität Heidelberg, Heidelberg, Germany, available at: http://www.ub.uni-heidelberg.de/archiv/5664/, 177 pp., 2005.

Kühl, S., Puķīte, J., Deutschmann, T., Platt, U., and Wagner, T.: SCIAMACHY Limb Measurements of NO_2, BrO and OClO, Retrieval of vertical profiles: Algorithm, first results, sensitivity and comparison studies, Adv. Space Res., 42, 1747–1764, 2008.

Platt, U. and Stutz, J.: Differential Optical Absorption Spectroscopy. Principles and Applications, in: Series: Physics of Earth and Space Environments, Springer, Heidelberg, 597 pp., doi:10.1007/978-3-540-75776-4, 2008.

Puķīte, J., Kühl, S., Deutschmann, T., Wilms-Grabe, W., Friedeburg, C., Platt, U., and Wagner, T.: Retrieval of stratospheric trace gases from SCIAMACHY limb measurements, Proceedings of the First Atmospheric Science Conference, 8–

12 May, ESA/ESRIN, Frascati, Italy, ESA SP-628, available at: http://earth.esa.int/workshops/atmos2006/participants/1148/paper_proc_Frasc_2.pdf (last access: 7 May 2010), 2006.

Puķīte, J., Kühl, S., Deutschmann, T., Platt, U., and Wagner, T.: Accounting for the effect of horizontal gradients in limb measurements of scattered sunlight, Atmos. Chem. Phys., 8, 3045–3060, doi:10.5194/acp-8-3045-2008, 2008.

Randel, W. J., Gille, J. C., Roche, A. E., Kumer, J. B., Mergenthaler, J. L., Waters, J. W., Fishbein, E. F., and Lahoz, W. A.: Stratospheric transport from the tropics to middle latitudes by planetary wave mixing, Nature, 365, 533–535, 1993.

Ridolfi, M., Magnani, L., Carlotti, M., and Dinelli, B. M.: MIPAS-ENVISAT Limb-Sounding Measurements: Trade-Off Study for Improvement of Horizontal Resolution, Appl. Optics, 43, 5814–5824, 2004.

Rodgers, C. D.: Inverse methods for atmospheric sounding, Theory and practice, World Scientific Publishing Co. Ltd., Singapore, 2000.

Rozanov, A., Bovensmann, H., Bracher, A., Hrechanyy, S., Rozanov, V., Sinnhuber, M., Stroh, F., and Burrows, J. P.: NO_2 and BrO vertical profile retrieval from SCIAMACHY limb measurements: Sensitivity studies, Adv. Space Res., 36(5), 846–854, doi:10.1016/j.asr.2005.03.013, 2005.

Russell, J. M., Tuck, A. F., Gordley, L. L., Park, J. H., Drayson, S. R., Harries, J. E., Cicerone, R. J., and Crutzen, P. J.: Haloe Antarctic observations in the spring of 1991, Geophys. Res. Lett., 20, 719–722, doi:10.1029/93GL00497, 1993

Sioris, C. E., Kovalenko, L. J., McLinden, C. A., Salawitch, R. J., Van Roozendael, M., Goutail, F., Dorf, M. Pfeilsticker, K., Chance, K., von Savigny, C., Liu, X., Kurosu, T. P., Pommereau, J.-P., Bösch, H., and Frerick, J.: Latitudinal and vertical distribution of bromine monoxide in the lower stratosphere from Scanning Imaging Absorption Spectrometer for Atmospheric Chartography limb scattering measurements, J. Geophys. Res., 111, D14301, doi:10.1029/2005JD006479, 2006.

Sioris, C. E., Kurosu, T. P., Martin, R. V., and Chance, K.: Stratospheric and tropospheric NO_2 observed by SCIAMACHY: First results, Adv. Space Res., 34, 780–785, 2004.

Steck, T., Höpfner, M., von Clarmann, T., and Grabowski, U.: Tomographic retrieval of atmospheric parameters from infrared limb emission observations, Appl. Optics, 44, 3291–3301, 2005

Trepte, C. R. and Hitchman, M. H.: Tropical stratospheric circulation deduced from satellite aerosol data, Nature, 355, 626–628, 1992

von Savigny, C., Rozanov, A., Bovensmann, H., Eichmann, K.-U., Noël, S., Rozanov, V. V., Sinnhuber, B.-M., Weber, M., and Burrows, J. P.: The ozone hole breakup in September 2002 as seen by SCIAMACHY on ENVISAT, J. Atmos. Sci., 62, 721–734, 2005.

Wagner, T., Burrows, J. P., Deutschmann, T., Dix, B., von Friedeburg, C., Frieß, U., Hendrick, F., Heue, K.-P., Irie, H., Iwabuchi, H., Kanaya, Y., Keller, J., McLinden, C. A., Oetjen, H., Palazzi, E., Petritoli, A., Platt, U., Postylyakov, O., Pukite, J., Richter, A., van Roozendael, M., Rozanov, A., Rozanov, V., Sinreich, R., Sanghavi, S., and Wittrock, F.: Comparison of box-air-mass-factors and radiances for Multiple-Axis Differential Optical Absorption Spectroscopy (MAX-DOAS) geometries calculated from different UV/visible radiative transfer models, Atmos. Chem. Phys., 7, 1809–1833, doi:10.5194/acp-7-1809-2007, 2007.